Supplementary material

Interfacial Bi–O–Zn bonding induces faster charge transfer in S-scheme Bi-MOF/$ZnFe_2O_4$ heterojunction for enhanced photocatalytic tetracycline elimination

Hui Li[a], Zhu Zhu[a], Kai Yang[a], Kang-Qiang Lu[a], Xi-Rong Chen[a], Wei-Ya Huang[a,*], Zhao-Qing Liu[b]

[a] *Jiangxi Provincial Key Laboratory of Functional Molecular Materials Chemistry, School of Chemistry and Chemical Engineering, Jiangxi University of Science and Technology, Ganzhou, 341000, PR China;*

[b] *School of Chemistry and Chemical Engineering/Institute of Clean Energy and Materials/Guangzhou Key Laboratory for Clean Energy and Materials/Huangpu Hydrogen Innovation Center, Guangzhou University, Guangzhou 510006, P. R. China.*

* Corresponding author:

Tel/Fax: +86(797) 8312334; E-mail addresses: hweiya@126.com (W-Y. Huang)

Contents

Text S1. Chemicals and reagents

Tetracycline hydrochloride (TC), bismuth nitrate pentahydrate ($Bi(NO_3)_3·5H_2O$), iron nitrate nonahydrate ($Fe(NO_3)_3·9H_2O$), zinc nitrate hexahydrate ($Zn(NO_3)_2·6H_2O$), p-benzoquinone, and ammonium oxalate were purchased from Shanghai Aladdin Biochemical Technology Co. Ethanol (≥99.70%) and methanol (≥99.50%) were provided by Xi-long Chemical Co. 1,3,5-benzoic acid (H_3BTC) and tert-butanol (TBA, ≥98.00%) were purchased from McLean Industrial Company, Shanghai, China. All reagents were of analytical grade, unless otherwise specified, and all solutions were prepared using deionized water.

S1.1 Synthesis of Bi-MOF

According to the literature, Bi-MOF was synthesized using an optimized synthetic method[1]. Initially, dissolve 0.75 g of H_3BTC and 0.15 g of $Bi(NO_3)_3·5H_2O$ in 60 mL of methanol to form a transparent solution. Rapidly pour this solution into a 100 mL PTFE-coated autoclave, and then heat it to 120 ℃ for a duration of 24 h. Once the temperature naturally decreases to 25 ℃, filter the mixture to collect a white solid. Thoroughly wash this solid three times with methanol to remove any residual impurities, and then dry it in a vacuum oven at a temperature of 70 ℃ for a period of 10 h. Finally, store the resulting sample in a sealed container for later use.

Text S2. Characteristics of materials

The composition, cellularity, and crystallinity of the materials were verified and analyzed using an X-ray powder diffractometer (XRD, Cu Kα, λ = 0.15406 nm, current: 40 mA, operating voltage: 40 kV). X-ray photoelectron spectroscopy (XPS, T Kα = 1486.6 eV, operating power: 100 W) was

employed to investigate the photocatalysts' elemental composition, content, chemical state, and molecular structure. Transmission electron microscopy (TEM, Tecnai F20, FEI, USA) was utilized to observe the particle size, shape, and lattice spacing of the catalysts. A scanning electron microscope (SEM, JSM-EG-250, FEI, USA) was used to examine the morphology, particle size, and elemental distribution of the samples. The functional groups and structures of the synthesized catalysts were elucidated using Fourier transform infrared spectroscopy with a DLATGS detector (FT-IR, Nicolet iS50, Thermo Scientific, USA). The specific surface area, pore size, and pore volume distribution of the materials were analyzed using a specific surface area analyzer (BET, ASAP 2020, Micromeritics Instrument Corporation, USA) based on the principle of nitrogen adsorption-desorption measurements. A UV-vis diffuse reflectance spectrophotometer (UV-vis DRS, Shimadzu UV-2600) was employed to analyze the light absorption properties of the materials, and the photoluminescence of the catalyst powder was measured using a fluorescence spectrophotometer (F-4500, Hitachi High-Technologies Corporation, Japan) The electron spin resonance (ESR) spectra were recorded on an electron spin resonance spectrometer (Bruker A300) in presence of visible light and without light 5,5-dimethyl-1-pyrroline N-oxide (DMPO: 50 mM, 0.2 mL) was used to capture ·OH and $\cdot O_2^-$ for ESR.

Text S3. Analysis and fitting of photodegradation efficiency data

The degradation efficiency of TC was calculated using the formula provided in Eq. (S1):

$$\eta = \frac{1-C}{Co} \times 100\% \quad \text{(S1)}$$

The initial concentration of the pollutant and the concentration at different times are expressed as C_o (mg/L) and C (mg/L)

A pseudo first order kinetic model for the photocatalytic degradation of pollutants as shown in Eq. (S2) ：

$$\ln\left(C/C_O\right) = -kt \tag{S2}$$

where C, C_o and k denote the concentration of the pollutant at time t, the initial concentration of the pollutant, and the apparent reaction rate constant, respectively.

The bandgap (E_g) represents the energy difference between the lowest energy level of the conduction band (CB) and the highest energy level of the valence band (VB) within the band structure, and it can be calculated using Eq.(S3) ：

$$\alpha h\upsilon = \left[A\left(h\upsilon - E_g\right)\right]^{\frac{n}{2}} \tag{S3}$$

Where h, α, E_g, A, and *v* are the Planck's constant, light absorption coefficient, bandgap energy, constant value, and optical frequency, respectively.

The standard potential can be calculated using this formula Eq.(S4):

$$E(\text{vs.NHE}) = E(\text{vs.Ag/AgCl}) + 0.22\text{eV}(\text{vs.NHE}, PH = 7) \tag{S4}$$

Text S4. Photoelectrochemical (PEC) Tests

The photoelectrochemical (PEC) test was conducted using an electrochemical workstation (CHI 760 e) in a conventional three-electrode cell system, which consisted of a working electrode with an exposed area of 2 × 1.5 cm^2, a saturated Ag/AgCl electrode as the reference electrode, and a Pt electrode as the counter electrode. The sample to be tested (10 mg) was mixed with 1 mL of ethanol and 30 μL of naphthol, and the mixture was sonicated for 20 min. The resulting suspension was used to uniformly coat FTO conductive glass and allowed to dry naturally. The three electrodes were

immersed in an electrolytic cell containing 20 mL of Na_2SO_4 solution (0.2 M). A 300 W xenon lamp was used, and a 420 nm filter was added to simulate sunlight with a power density of 150 m W cm^{-2}. Electrochemical impedance spectra (EIS), transient photocurrent response (i-t), and Mott-Schottky (M-S) curves were characterized using an electrochemical system, CHI 660D (Chenhua Instrument Co., Ltd., Shanghai, China).

Text S5. TC degradation pathways

The degradation intermediates of TC were identified through liquid chromatography-mass spectrometry. The method employed included an electrospray ionization (ESI) source with parameters set as follows: spray voltage of 3.2 kV, capillary temperature at 300 °C, maximum spray current of 100 μA, and a probe heater temperature of 300 °C. The mobile phases consisted of methanol and 0.1% formic acid in water for gradient elution. The mass spectrometry analysis was conducted in negative ion mode, scanning the m/z range from 100 to 1000.

Fig. s：

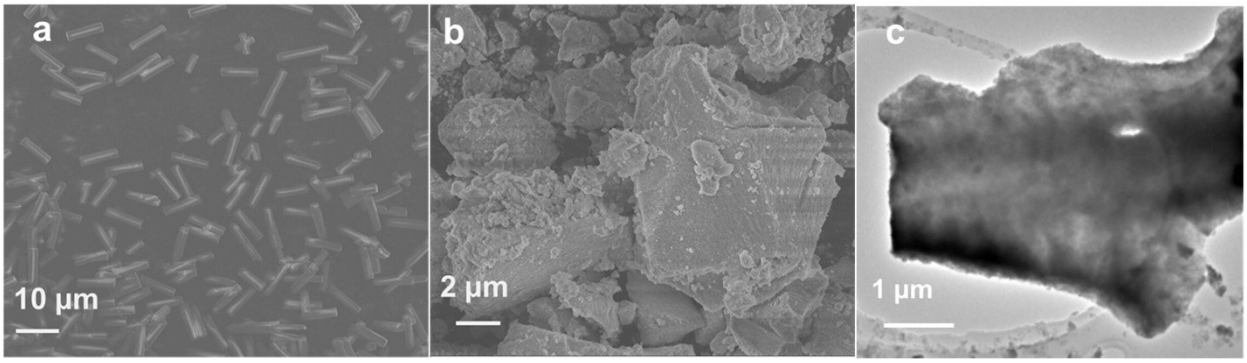

Fig. S1. SEM images s of (a) Bi-MOF, and (b) $ZnFe_2O_4$; (c) TEM image of $ZnFe_2O_4$.

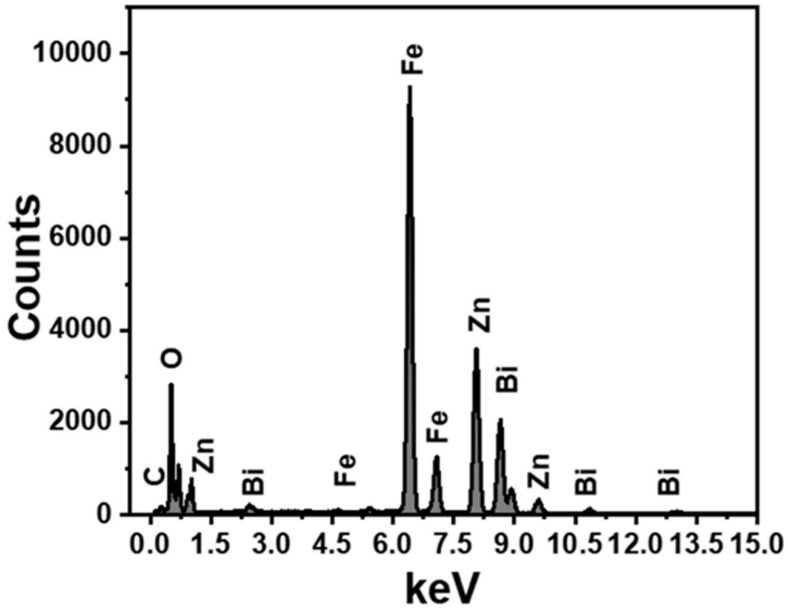

Fig. S2. elemental mapping image of ZFB-2.

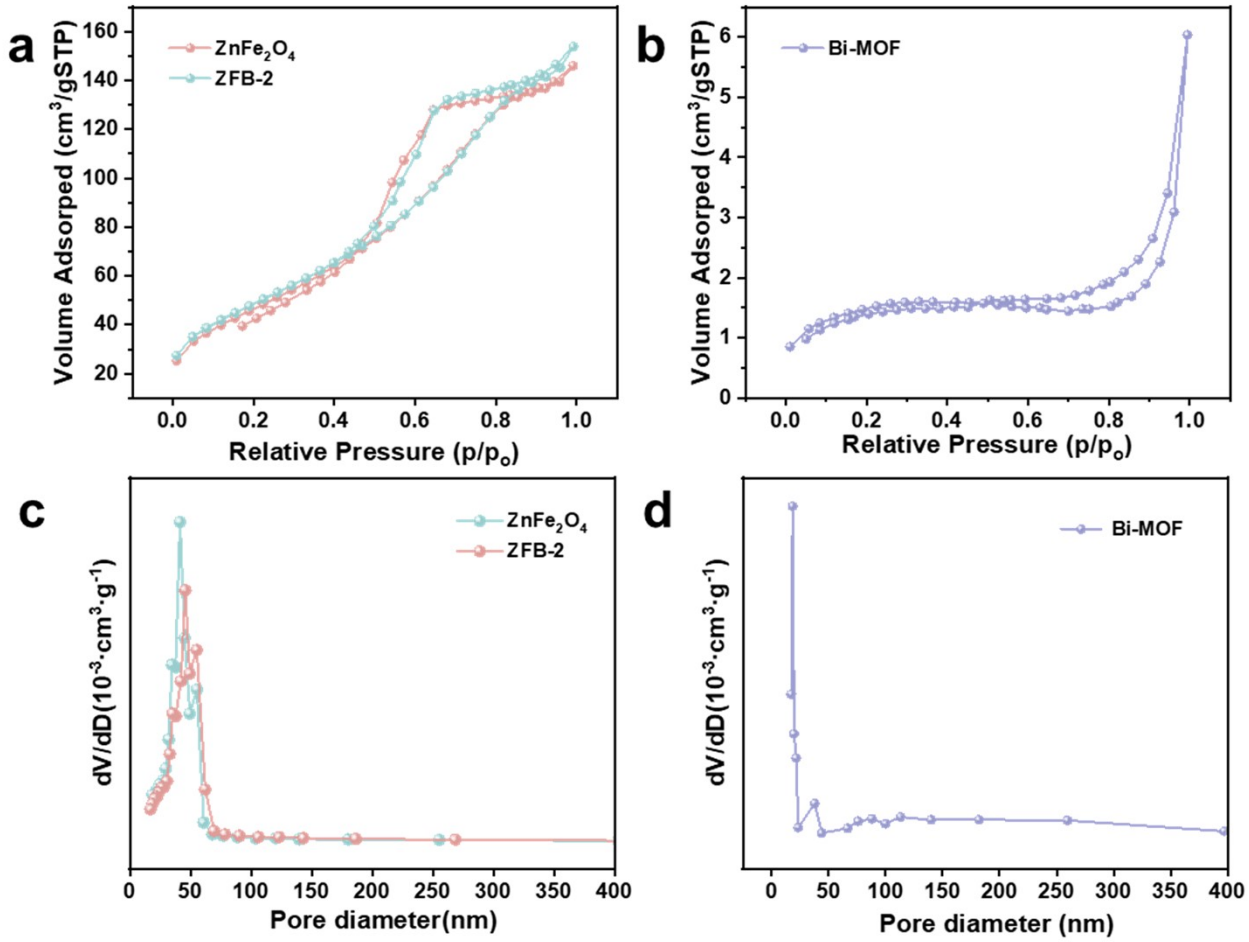

Fig. S3. (a-b) N_2 adsorption-desorption isotherm curves, and (c-d) pore size distribution plots of $ZnFe_2O_4$, ZFB-2, and Bi-MOF.

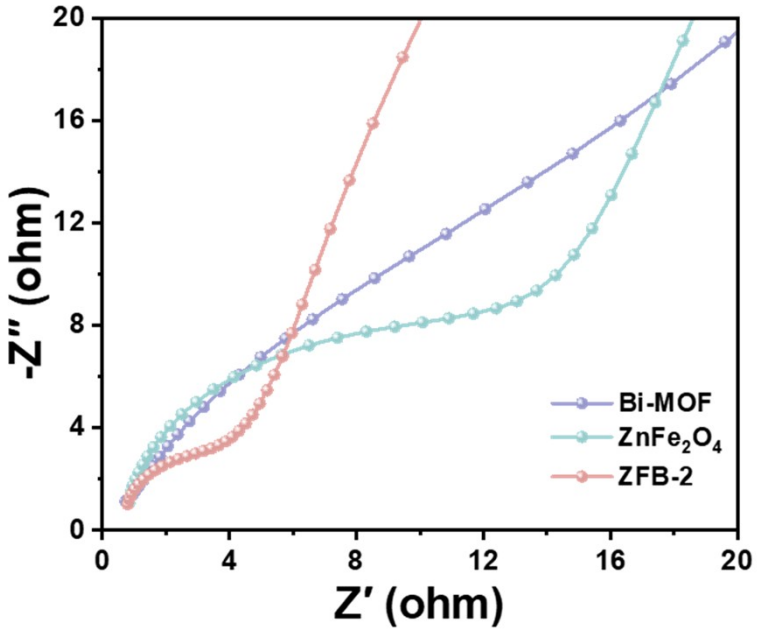

Fig. S4. Nyquist impedance plots of the sample.

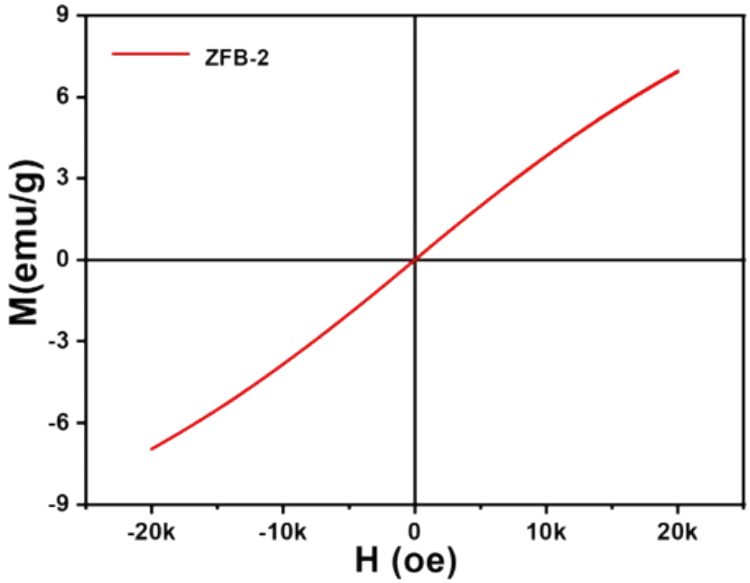

Fig.S5. Magnetization curves of ZFB-2 measured at room temperature.

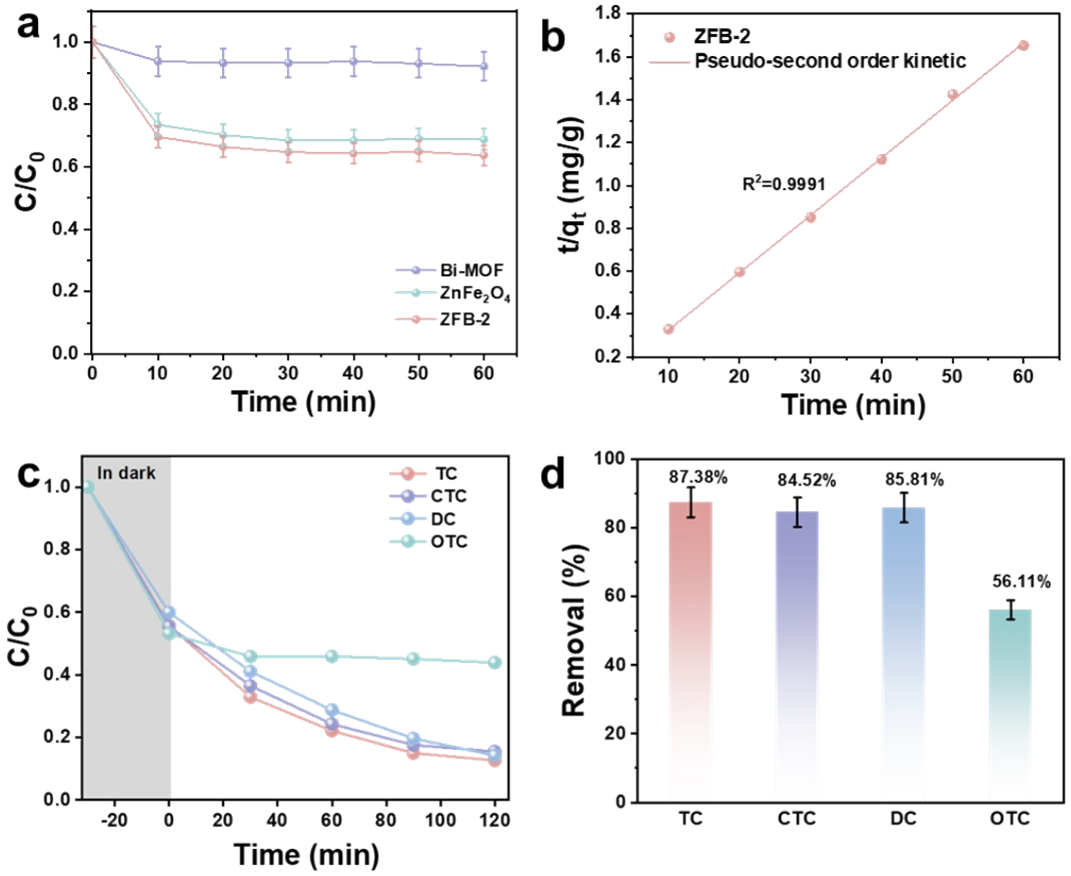

Fig. S6. (a) Adsorption of TC over Bi-MOF, $ZnFe_2O_4$, and ZFB-2 in dark; (b) Pseudo-second order kinetic fitting of ZFB-2; (c-d) degradation of other antibiotic pollutants in wastewater by ZFB-2.

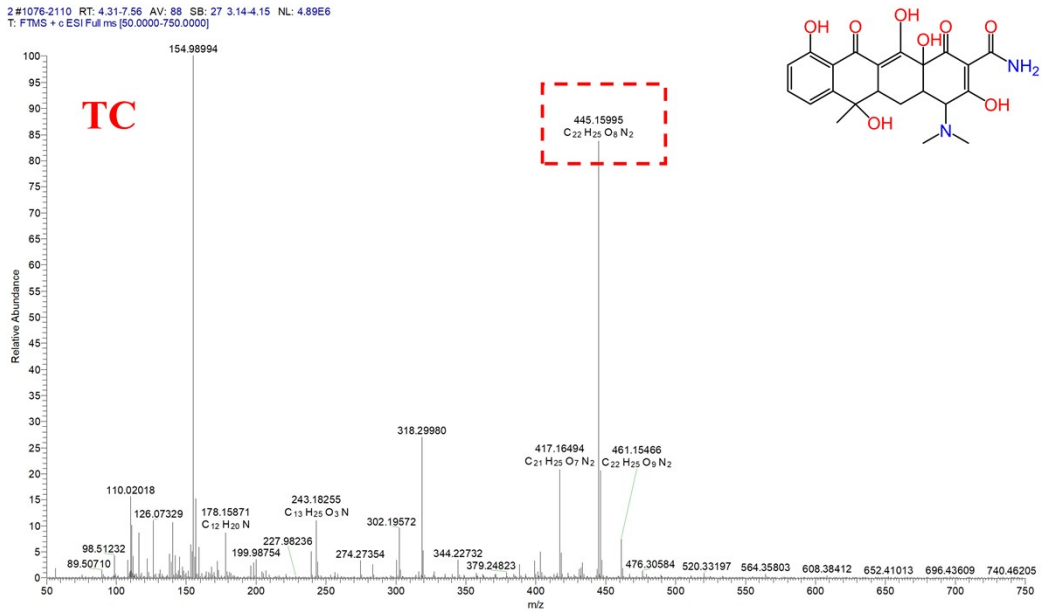
2 #1076-2110 RT: 4.31-7.56 AV: 88 SB: 27 3.14-4.15 NL: 4.89E6
T: FTMS + c ESI Full ms [50.0000-750.0000]
TC
445.15995
C22 H25 O8 N2
154.98994
318.29980
417.16494
C21 H25 O7 N2
461.15466
C22 H25 O9 N2
110.02018
126.07329
178.15871
C12 H20 N
243.18255
C13 H25 O3 N
302.19572
227.98236
199.98754
274.27354
344.22732
379.24823
98.51232
89.50710
476.30584
520.33197
564.35803
608.38412
652.41013
696.43609
740.46205
Relative Abundance
m/z

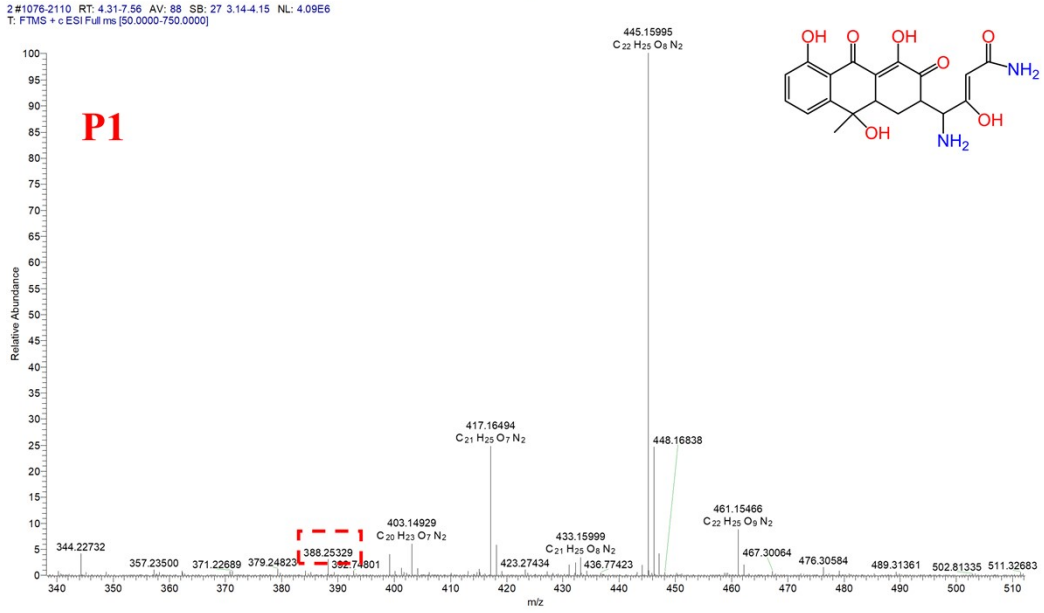
2 #1076-2110 RT: 4.31-7.56 AV: 88 SB: 27 3.14-4.15 NL: 4.09E6
T: FTMS + c ESI Full ms [50.0000-750.0000]
P1
445.15995
C22 H25 O8 N2
417.16494
C21 H25 O7 N2
448.16838
461.15466
C22 H25 O9 N2
403.14929
C20 H23 O7 N2
433.15999
C21 H25 O8 N2
344.22732
357.23500
371.22689
379.24823
388.25329
392.74801
423.27434
436.77423
467.30064
476.30584
489.31361
502.81335
511.32683
Relative Abundance
m/z

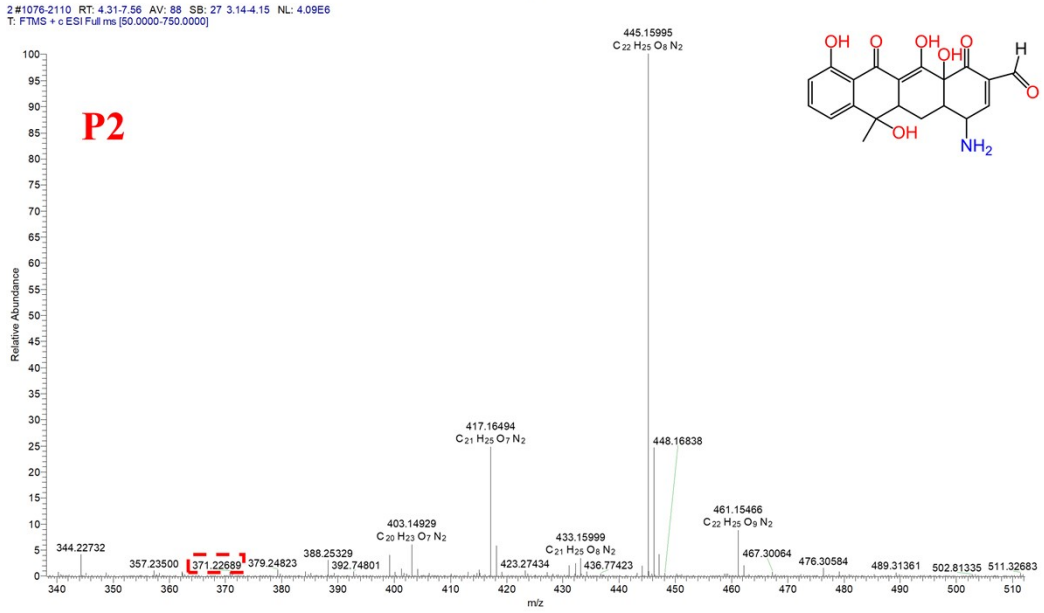
2 #1076-2110 RT: 4.31-7.56 AV: 88 SB: 27 3.14-4.15 NL: 4.09E6
T: FTMS + c ESI Full ms [50.0000-750.0000]
P2
445.15995
C22 H25 O8 N2
417.16494
C21 H25 O7 N2
448.16838
461.15466
C22 H25 O9 N2
403.14929
C20 H23 O7 N2
433.15999
C21 H25 O8 N2
344.22732
357.23500
371.22689
379.24823
388.25329
392.74801
423.27434
436.77423
467.30064
476.30584
489.31361
502.81335
511.32683
Relative Abundance
m/z

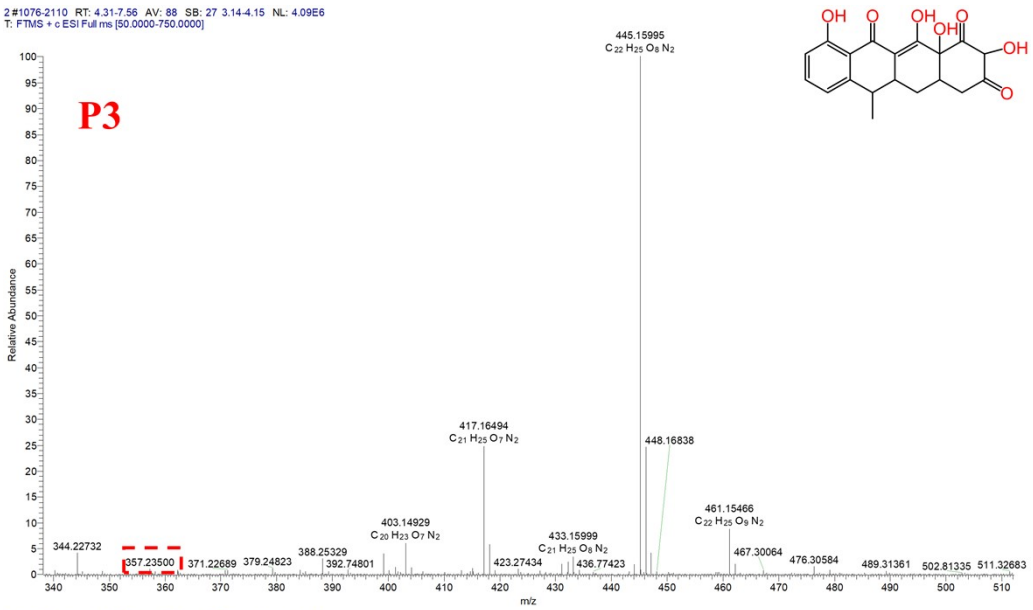
2 #1076-2110 RT: 4.31-7.56 AV: 88 SB: 27 3.14-4.15 NL: 4.09E6
T: FTMS + c ESI Full ms [50.0000-750.0000]
P3
445.15995
C22 H25 O8 N2
417.16494
C21 H25 O7 N2
448.16838
461.15466
C22 H25 O9 N2
403.14929
C20 H23 O7 N2
433.15999
C21 H25 O8 N2
344.22732
357.23500
371.22689
379.24823
388.25329
392.74801
423.27434
436.77423
467.30064
476.30584
489.31361
502.81335
511.32683
Relative Abundance
m/z

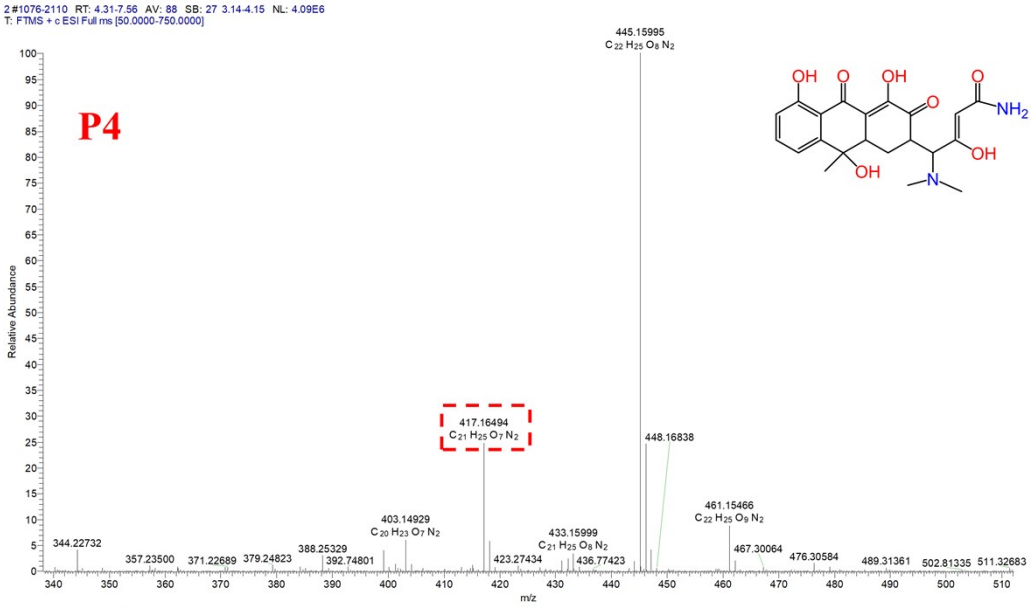
2 #1076-2110 RT: 4.31-7.56 AV: 88 SB: 27 3.14-4.15 NL: 4.09E6
T: FTMS + c ESI Full ms [50.0000-750.0000]
P4
445.15995
C22 H25 O8 N2
417.16494
C21 H25 O7 N2
448.16838
461.15466
C22 H25 O9 N2
403.14929
C20 H23 O7 N2
433.15999
C21 H25 O8 N2
344.22732
357.23500
371.22689
379.24823
388.25329
392.74801
423.27434
436.77423
467.30064
476.30584
489.31361
502.81335
511.32683
Relative Abundance
m/z

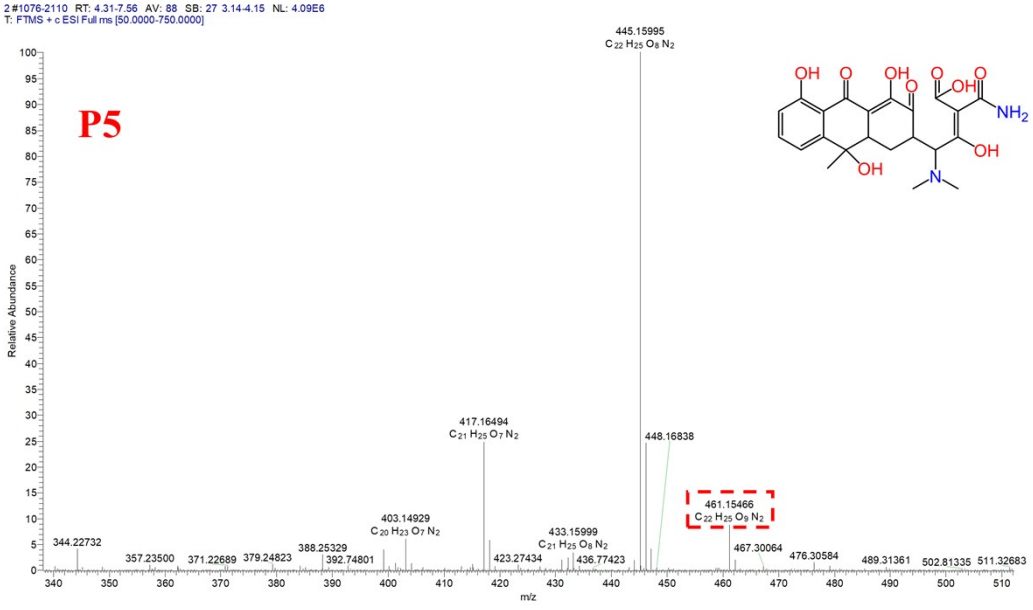
2 #1076-2110 RT: 4.31-7.56 AV: 88 SB: 27 3.14-4.15 NL: 4.09E6
T: FTMS + c ESI Full ms [50.0000-750.0000]
P5
445.15995
C22 H25 O8 N2
417.16494
C21 H25 O7 N2
448.16838
461.15466
C22 H25 O9 N2
403.14929
C20 H23 O7 N2
433.15999
C21 H25 O8 N2
344.22732
357.23500
371.22689
379.24823
388.25329
392.74801
423.27434
436.77423
467.30064
476.30584
489.31361
502.81335
511.32683
Relative Abundance
m/z

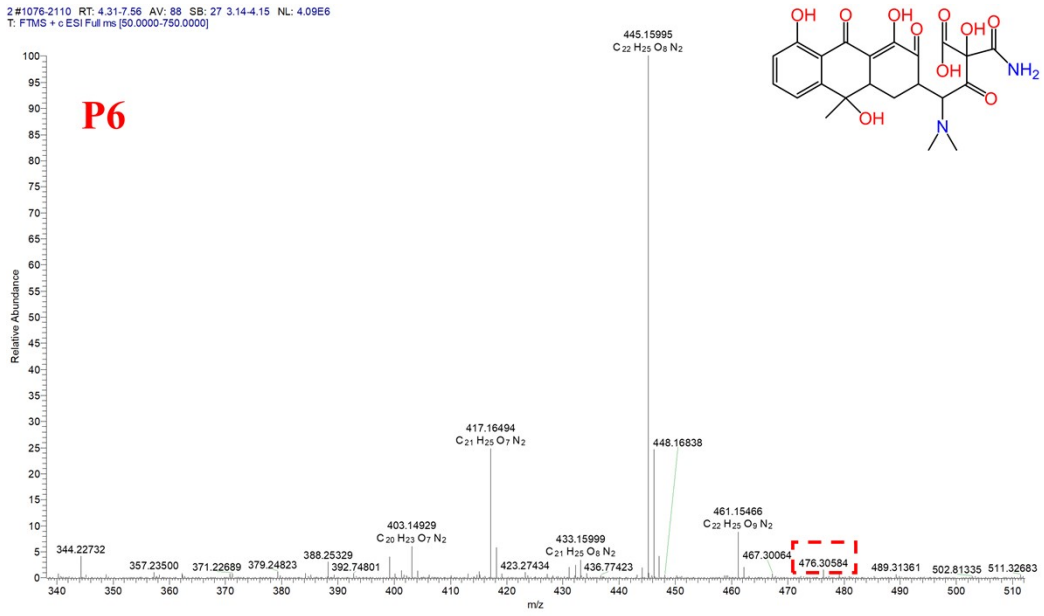
2 #1076-2110 RT: 4.31-7.56 AV: 88 SB: 27 3.14-4.15 NL: 4.09E6
T: FTMS + c ESI Full ms [50.0000-750.0000]
P6
445.15995
C22 H25 O8 N2
417.16494
C21 H25 O7 N2
448.16838
461.15466
C22 H25 O9 N2
403.14929
C20 H23 O7 N2
433.15999
C21 H25 O8 N2
344.22732
357.23500
371.22689
379.24823
388.25329
392.74801
423.27434
436.77423
467.30064
476.30584
489.31361
502.81335
511.32683
Relative Abundance
m/z

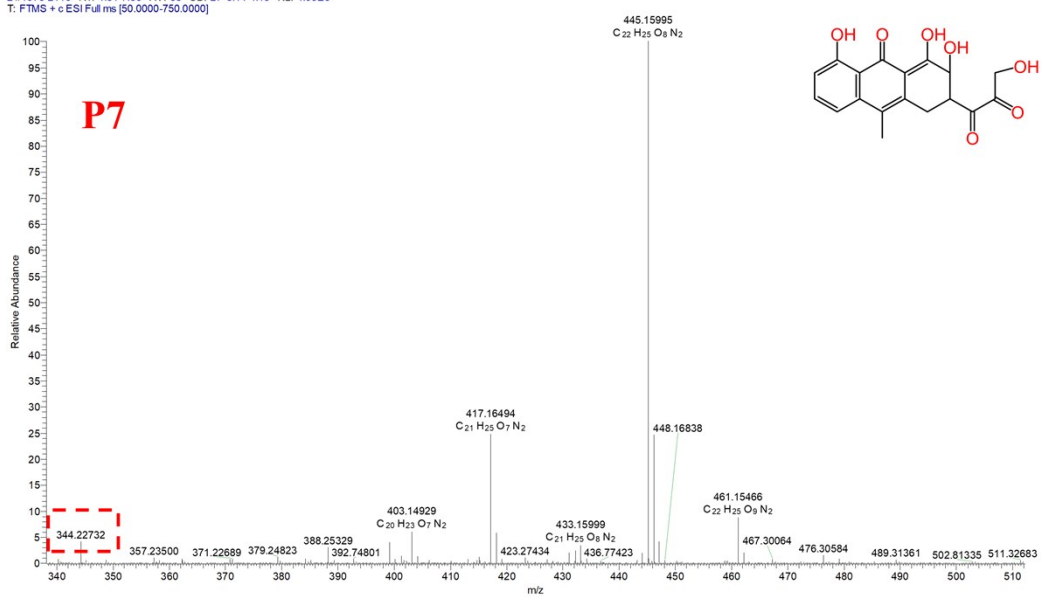
2 #1076-2110 RT: 4.31-7.56 AV: 88 SB: 27 3.14-4.15 NL: 4.09E6
T: FTMS + c ESI Full ms [50.0000-750.0000]
P7
445.15995
C22 H25 O8 N2
417.16494
C21 H25 O7 N2
448.16838
461.15466
C22 H25 O9 N2
403.14929
C20 H23 O7 N2
433.15999
C21 H25 O8 N2
344.22732
357.23500
371.22689
379.24823
388.25329
392.74801
423.27434
436.77423
467.30064
476.30584
489.31361
502.81335
511.32683
Relative Abundance
m/z

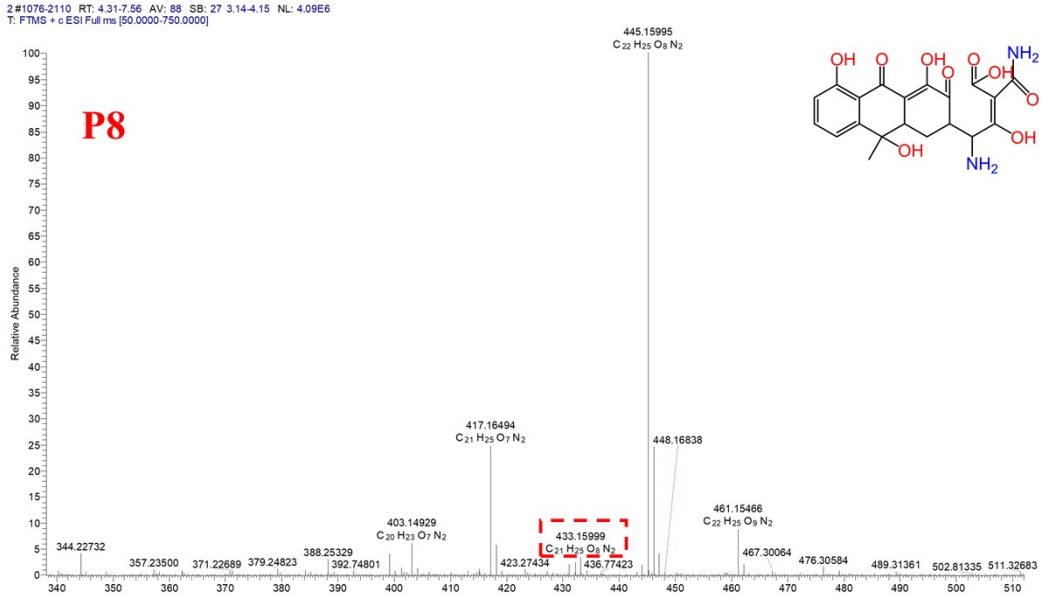
2 #1076-2110 RT: 4.31-7.56 AV: 88 SB: 27 3.14-4.15 NL: 4.09E6
T: FTMS + c ESI Full ms [50.0000-750.0000]
P8
445.15995
C22 H25 O8 N2
417.16494
C21 H25 O7 N2
448.16838
461.15466
C22 H25 O9 N2
403.14929
C20 H23 O7 N2
433.15999
C21 H25 O8 N2
344.22732
357.23500
371.22689
379.24823
388.25329
392.74801
423.27434
436.77423
467.30064
476.30584
489.31361
502.81335
511.32683
Relative Abundance
m/z

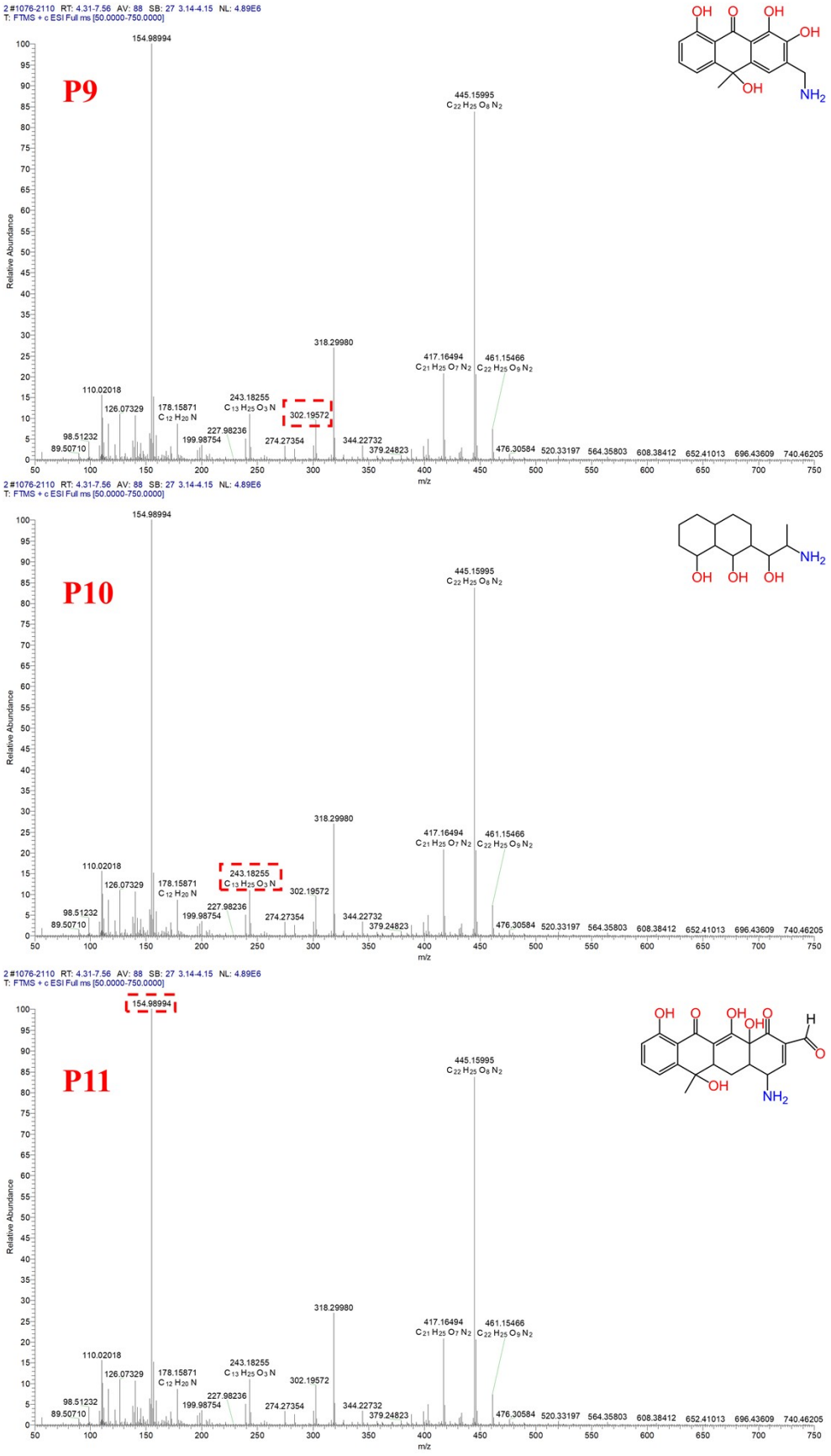

Fig. S7. HPLC-MS spectroscopy of TC during photocatalytic degradation Tables.

Tables:

Table S1: Specific surface area, average pore size and pore volume of Bi-MOF, $ZnFe_2O_4$ and ZFB-2.

Samples	Specific surface area (m^2/g)	Average pore size (nm)	Pore volume (cm^3/g)
Bi-MOF	5.01	74.47	0.0093
$ZnFe_2O_4$	172.43	52.39	0.23
ZFB-2	178.00	53.47	0.24

Table S2: First-order kinetic rate constants and correlation coefficients for the degradation of TC by the prepared samples.

Samples	k (min^{-1})	R^2
Bi-MOF	0.0003	0.79307
$ZnFe_2O_4$	0.00668	0.99791
ZFB-1	0.00799	0.99727
ZFB-2	0.01252	0.97301
ZFB-3	0.00888	0.99853
ZFB-4	0.00917	0.98238

Table S3: Comparison of photocatalytic degradation efficiency with other MOF-based photocatalysts.

Catalysts	Target pollutant (g/L)	Removal efficiency (time: min)	Catalyst capacity (g/L)	Ref.
CAU-17-0.02S	TC (0.020)	62.90% (120)	0.25	[2]
MoS_2/ZIF-8	TC (0.020)	75.60% (180)	0.4	[3]
Bi_2O_3/Fe-MOF-3	TC (0.010)	88.42% (120)	0.1	[4]
MoS_2/UiO-66	TC (0.020)	86.60 % (120)	0.5	[5]
ZFB-2	TC (0.010)	87.38% (120)	0.1	This work

Table S4: Comparison of photocatalytic degradation efficiency with other catalysts at pH = 7

Catalysts	Optimal pH	Removal efficiency	Ref.
MoS_2/UiO-66	7	86.60%	[5]
40RGO-CdTe	7	83.6%	[6]
15%-g-C_3N_4/Bi_5O_7I	7	98.7%	[7]
ZFB-2	7	87.38%	This work

Table S5: First-order kinetic rate constants and correlation coefficients for cycling test of ZFB-2 photocatalytic degradation of TC.

Cycle times	k (min^{-1})	R^2
1st	0.01228	0.99284
2nd	0.01206	0.99183
3rd	0.01112	0.98126
4th	0.01011	0.95147
5th	0.00924	0.96413

References

1 A. K. Inge, M. Köppen, J. Su, M. Feyand, H. Xu, X. Zou, M. O'Keeffe and N. Stock, Unprecedented Topological Complexity in a Metal–Organic Framework Constructed from Simple Building Units, *Journal of the American Chemical Society*, 2016, **138**, 1970-1976. DOI: 10.1021/jacs.5b12484.

2 M. Chen, S. Wei, J. Wu, J. Li, B. Fu and X. Zhu, Sulfur doped Bi-MOF with adjustable band gap for tetracycline removal under visible light, *Colloids and Surfaces A: Physicochemical and Engineering Aspects*, 2023, **664**, 131186. DOI: 10.1016/j.colsurfa.2023.131186.

3 W.-Q. Chen, L.-Y. Li, L. Li, W.-H. Qiu, L. Tang, L. Xu, K.-J. Xu and M.-H. Wu, MoS2/ZIF-8 Hybrid Materials for Environmental Catalysis: Solar-Driven Antibiotic-Degradation

Engineering, *Engineering*, 2019, **5**, 755-767. DOI: 10.1016/j.eng.2019.02.003.

4 A. Sharma, M. Tahir, T. Ahamad, N. Kumar, S. Sharma, M. Kumari, M. A. Majeed Khan, S. Takhur and P. Raizada, Improved charge transfer and enhanced visible light photocatalytic activity of Bi_2O_3@Fe-MOF for degradation of Rhodamine B and Triclopyr, *Journal of King Saud University - Science*, 2023, **35**, 102922. DOI: 10.1016/j.jksus.2023.102922.

5 Y. Gao, W. Yang, F. Wang, Y. Li, S. Cui, X. Liao and J. Yang, Photocatalytic degradation of oxytetracycline by UiO-66 doped three-dimensional flower-like MoS_2 heterojunction: DFT, degradation pathways, mechanism, *Journal of the Taiwan Institute of Chemical Engineers*, 2023, **152**, 105160. DOI: 10.1016/j.jtice.2023.105160.

6 S. Ghosh, K. Chakraborty, T. Pal and S. Ghosh, Photocatalytic degradation of tetracycline antibiotics by RGO-CdTe composite with enhanced apparent quantum efficiency, *Scientific Reports*, 2023, **13**, 19028. DOI: 10.1038/s41598-023-46120-0.

7 D. Tan, F. Huang, S. Guo, D. Li, Y. Yan and W. Zhang, Efficient photocatalytic tetracycline elimination over Z-scheme g-C_3N_4/Bi_5O_7I heterojunction under sunshine light: Performance, mechanism, DFT calculation and pathway, *Journal of Alloys and Compounds*, 2023, **946**, 169468. DOI: 10.1016/j.jallcom.2023.169468.